GPR full waveform inversion for chlorides and moisture detection in concrete

A. Kalogeropoulos, J. Hugenschmidt
Swiss Federal Laboratories for Materials Testing and
Research, EMPA
Ueberlandstrasse 129 , 8600, Duebendorf, Switzerland
alexis.kalogeropoulos@empa.ch,
johannes.hugenschmidt@empa.ch

J. van der Kruk, K. Merz
formerly ETH Zurich switzerland
now at Forschungszentrum Juelich
Agrosphere ICG4, 52425, Juelich, Germany
j.van.der.kruk@fz-juelich.de

Abstract—**Corrosion of rebar within reinforced concrete is a major problem for countries where salt is applied to roads for de-icing. Concrete structures are periodically inspected in order to monitor possible damage caused by chloride-induced corrosion of the reinforcement. However, the available drilling and visual inspection do not supply sufficient spatial information or can only be assessed in advanced stages of corrosion, respectively. Consequently, the condition of bridge decks can only be assessed with low certainty. Therefore a spatially continuous and non-destructive method detecting chloride gradients in concrete structures is desirable. This paper describes processing strategies for material properties evaluation using a full waveform inversion algorithm. The results provide estimates of the quantitative electromagnetic properties of nine concrete specimens having different chloride and moisture contents and show that increased chloride contents have a stronger influence on electromagnetic wave propagation than increased humidity.**

Index —**Concrete structures, Chloride content, Reinforcement corrosion, Non-destructive testing, Ground Penetrating Radar, Full waveform inversion.**

I. INTRODUCTION

In many countries salt is applied on roads for de-icing. Due to alternating weathering cycles the chloride dissolved in the melt water on bridge decks gradually migrates through the pores of the concrete by diffusion and capillarity. Once the depth of reinforcing bars (rebars) is reached (up to 4cm), chlorides lower the pH of surrounding concrete, remove the passivation layer at the steel-concrete interface and cause the initiation of corrosion processes. The corroded rebars increase in volume and cause cracking and delamination of the concrete. Once corroded, the reinforcement looses its mechanical properties and this can lead to structural failure.

Civil engineers usually detect these corrosion processes by visual inspection (observation of cracks and rust deposits); and total chloride content chemical measurement of drilled cores. Three limitations are present in this assessment methodology, 1) visual inspection requires corrosion process being in an advanced stage to observe their manifestations; 2) core drilling is punctual and destructive. In addition, 3) bridge decks covered with asphalt are not accessible for visual inspection. Therefore a continuous and non-destructive method detecting chloride gradients in concrete structures is needed.

For such assessments, Ground penetrating radar GPR presents two important advantages: first, it allows keeping the structure open for traffic during its inspection; second, the device can locate changes of medium conditions.

Electromagnetic waves propagation in concrete depends on its electromagnetic characteristics, e.g. conductivity σ and the relative dielectric permittivity ε, which are dominantly influenced by chloride and water content, respectively.

The Swiss Federal Laboratories for Materials Testing and Research, EMPA in Duebendorf, Switzerland, performed GPR measurements on nine concrete specimens with fixed chloride content and controlled moisture content [1]. Results have shown that amplitudes of reflections are influenced by both the chloride and moisture content. It was found that the quotient between the reflected amplitudes of the concrete surface and an aluminum sheet situated below the specimens is a possible qualitative approach for moisture and chloride detection. However, it was not possible to discriminate between moisture and chloride and they were detected qualitatively.

Recently, several full-waveform inversions have been developed that enable medium properties quantitative estimation by fitting the whole measured waveform with an accurate forward model [2]-[5].

This paper describes processing of the EMPA data using a full- waveform inversion which renders quantitative estimations of conductivity and dielectric permittivity for each specimen.

II. MEASUREMENT SETUP

The measurement setup consists of two off-ground 1.2 GHz horn antennas with an offset of 0.28 m (Fig. 1). Measurements were carried out over a 0.08 m thick concrete slab overlying an aluminium plate. In this way, two reflections were measured, one coming from the air-concrete interface and one coming from the concrete-aluminium interface.
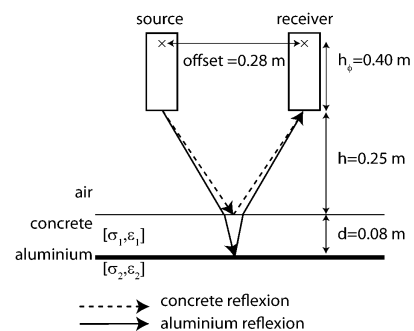

Fig. 1. Measurement setup

III. FORWARD MODEL

A. Medium properties

Several authors have assessed frequency dependent conductivity [6], [7]. Similar to [2], the analysis of the measured data revealed that for high chloride contents the high frequencies contained lower amplitudes. Therefore, the conductivity was assumed to be frequency dependent according to

$$\sigma(f) = \sigma_{fc} + k \frac{(f - f_c)}{f_c}, \tag{1}$$

where f_c is the center frequency of the GPR system, σ_{fc} is the reference electric conductivity at the center frequency and k is the linear variation rate of $\sigma(f)$. The dielectric permittivity was assumed to be frequency independent.

B. Greens function

To perform a full-waveform inversion of this data, an accurate forward model that describes the propagation of electromagnetic waves is necessary. In this way, the wave propagation from the source antenna to the concrete slab, both reflections coming from the air-concrete and concrete aluminum interface and the back-propagating wave to the receiver again are modeled (Fig. 1). Similar to [2], [8], a Greens function $\hat{G}$ that describes these events in frequency domain for a horizontally layered medium is introduced:

$$\hat{E}_{model}(f) = \hat{G}(f, \varepsilon_r, \sigma_{fc}, k) \cdot \hat{W}(f), \tag{2}$$

where $\hat{W}$ is the effective wavelet that contains the influence of the source and receiver antennas. The Green function can be divided into

$$\hat{G}(f, \varepsilon_r, \sigma_{fc}, k) = \hat{G}^{ac}(f, \varepsilon_r, \sigma_{fc}, k) \\ + \hat{G}^{ca}(f, \varepsilon_r, \sigma_{fc}, k), \tag{3}$$

where $\hat{G}^{ac}$ and $\hat{G}^{ca}$ describe the propagation of the first reflection on the air-concrete interface and the second reflection of the concrete-aluminum interface, respectively. The antennas are modeled as point sources and their central frequency is to 1.2 GHz. Note, that the Greens function depends on three parameters that will be optimized in the inversion procedure.

IV. ANTENNA CALIBRATION

A. Phase center estimation

To estimate both antenna's phase center, calibration measurements were carried out having the horn antennas over a moving metal plate for heights h varying between 0.1<h<0.65 m (Fig.1). This estimation was done by extrapolating the inverse values of the maximum, minimum-maximum and energy values of the reflected waveforms towards zero amplitude (Fig. 2). All three estimates returned a similar value of $h_\phi = 0.40$ m, which was regarded as the phase center of the horn antennas.
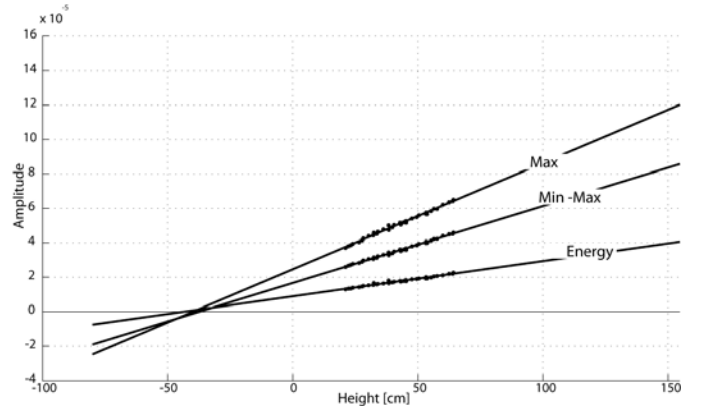

Fig. 2. Linear regression using the inverse values of reflected calibration waveforms values (maximum, minimum-maximum and energy).

B. Effective wavelet estimation

The effective wavelet was extracted for each specimen by spectral division of the measured data and the Greens function:

$$\hat{W}(f) = \frac{\hat{E}_{data}(f)\hat{G}^*(f)}{\hat{G}(f)\hat{G}^*(f) + 10^{-8}}, \tag{4}$$

where $\hat{E}_{data}(f)$ are the calibration measurements over a specific reference metal plate for a fixed height. $\hat{G}(f)^*$ is the complex conjugate of $\hat{G}(f)$, the calculated green's function of the system assuming a total reflection of the incident wave on the aluminum surface (reflection coefficient equals -1), and the value 10^{-8} is used for water level regularization.

C. Inversion

After estimating the phase center and the effective wavelet, GPR measurements are modeled using (2) and the parameters ε_r, σ_{fc} and k are optimized to fit the modeled data with real data by minimizing the following cost function:

$$C(\varepsilon_r, \sigma_{fc}, k) = \sum_{i=1}^{n} \frac{\left| \hat{E}_{data}(f_i) - \hat{E}_{model}(f_i) \right|}{n}. \tag{5}$$

This inversion is carried out using a combined global and local optimization algorithm that performs for different starting values a local minimization based on the simplex search algorithm [9].

Two consecutive inversions were carried out. The first one inverts only the bottom concrete-aluminum interface reflection and the second considers both the air-concrete and concrete-aluminum interface reflections (Fig. 1).

V. EXPERIMENTAL SETUP

Nine concrete slabs were produced [1], each with dimensions of 0.90 m, 0.75 m, 0.08 m. Three concrete mixtures with maximum aggregate size of 32 mm, constant volume of paste but different chloride content were used (Table 1). Chlorides were added to the mixtures by dissolving NaCl in the mixing water. A chloride content of 0.4% is the upper limit accepted under normal circumstances in civil engineering. All mixtures had comparable fresh concrete properties. The concrete was cast in three moulds per mixture.

Table 1. Specimen numeration.

Moisture	Chloride		
	0.0%	0.4%	1.0%
90%	4	5	6
70%	1	2	3
35%	7	9	8

The base of the moulds where covered with aluminum sheets. After compaction, the specimens were stored at 20°C and 90% relative humidity (r.h.) for 2 days. Afterwards, one specimen of each mixture was moved to climates of 35% r.h., 70% r.h. and 90% r.h. for 99 days before the radar measurements were carried out. One would expect to obtain increasing dielectric permittivity ε for increasing water content and increasing conductivity σ for increasing chloride content

VI. RESULTS

A. Inverted waveforms assessment

The following discussion will focus on the results of the inversion of both reflections since the first inversion (bottom concrete-aluminum) returned similar results. The solid line in Fig. 3 shows a characteristic measured trace containing two reflections coming from both interfaces. The inverted trace indicated by the dotted line is similar as the measured trace. It was observed for all specimens that the second reflection inversion gives a better fit in amplitudes than the first reflection.

Fig. 4 shows the corresponding phase and frequency information of both traces, which is actually what is inverted for using (5). One can see that the fit is optimal in both plots, around the horn antennas central frequency f_c=1.2 GHz.
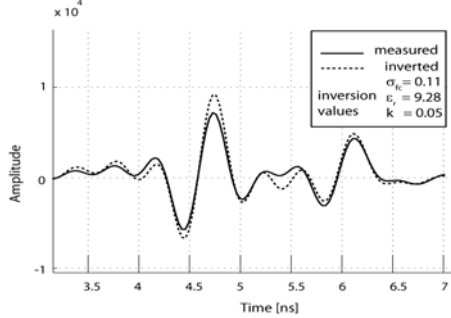

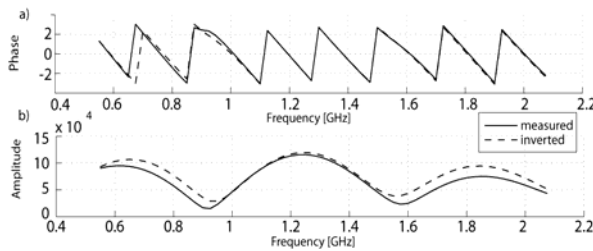Fig. 3. Time domain plots of measured and inverted data (specimen 3).

Fig. 4. a) Phase and b) amplitude of measured and inverted data shown in Fig 3 (specimen 3).

B. Inverted conductivity and relative dielectric permittivity

In the following, we will present inversion results by plotting the obtained medium properties as function of the relative humidity and chloride content to investigate their influence.

Fig. 6 shows that for increasing chloride content a larger conductivity is obtained. The relative humidity has little influence on the conductivity values.
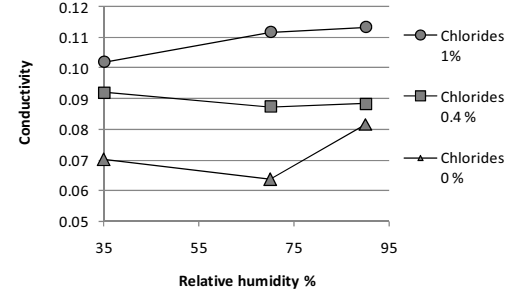

Fig. 6. Inverted conductivity values as function of the relative humidity for different chloride contents.

Fig. 7 shows the obtained relative permittivity as a function of the relative humidity for the different chloride contents. The identical chloride content series show moderately increasing relative permittivity values for increasing relative humidity. Note the slight increase in relative permittivity for increasing humidity compared to the significant increase in conductivity for increasing chloride content.
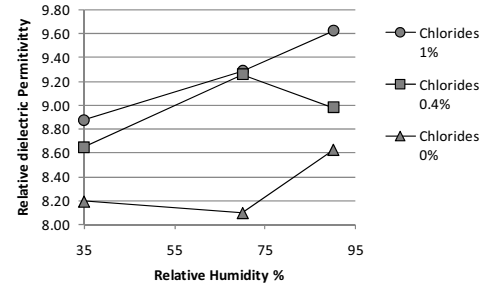

Fig. 7. Inverted relative permittivity values as function of the relative humidity for different chloride content specimen.

Fig. 8 shows that conductivity is strongly increasing for increasing chloride content, and that the slopes are similar for the three different relative humidities.
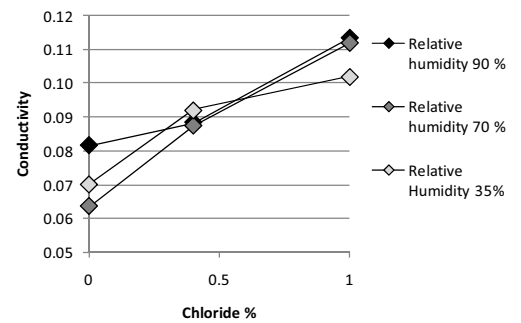

Fig. 8. Inverted conductivity values as function of the chloride content for the different relative humidity specimen

Fig. 9 shows in general an increase of the inverted relative permittivity for increasing chloride content for the different relative humidities.

In previous figures three outliers could be identified which did not follow the expected trend; specimen 2 (70% relative humidity and 0.4% chloride), specimen 7 (35% relative humidity and 0% chlorides) and specimen 9 (35% relative humidity and 1% chloride). These outliers will be investigated in more detail. Probably using a similar calibration procedure as [2], and optimizing the frequency range will improve the inversion results.
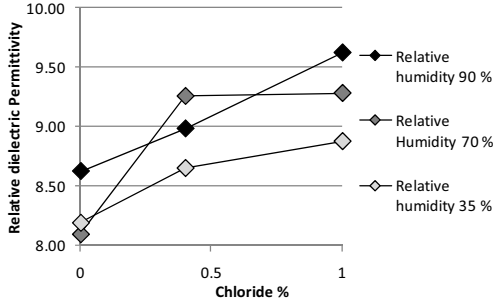

Fig. 9. Inverted relative permittivity values as function of the chloride content for different values of relative humidity specimen.

Fig. 10 shows an overview of all the specimen as function of conductivity and relative permittivity. Again, for increasing chloride and humidity an increasing conductivity and permittivity can be observed, respectively. In this way, both relative humidity and chloride content effects can be observed. The three outliers (specimens 2, 7, 9, Table 1) previously identified are indicated in Fig.10.

These figures show that the chloride content has a stronger effect on conductivity values than relative humidity has on relative permittivity. Moreover, increasing chloride content has similar influence than relative humidity on relative dielectric permittivity values. This demonstrates that chloride content is a more discriminating parameter than relative humidity on electromagnetic wave propagation in concrete.
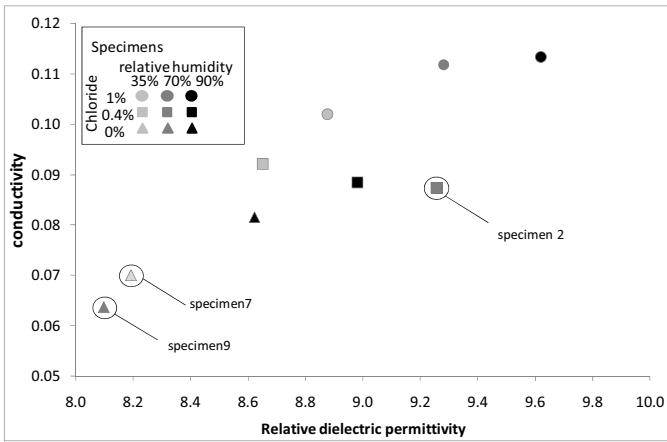

Fig. 10. Relative dielectric permittivity and relative conductivity values of all specimens.

C. Inverted frequency dependent relative conductivities

Fig 11 plots the linear frequency dependent conductivities

(1) for all inverted specimens (Table 1). It is observed that the 1% chloride results (circles) have the steepest slopes and the highest relative conductivity values. Squares (0.4% chlorides) have intermediates slopes and medium σ values. Finally, triangles (0% chlorides) show flat and inverse (0% chloride) slopes with low σ values. Note that two aforementioned outliers (specimen 7&9) correspond to the inverse and flat slope, respectively.
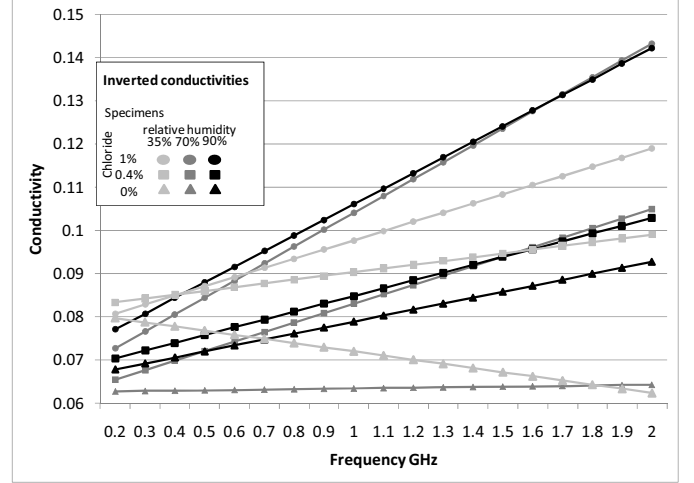

Fig. 11. Inversion results of frequency dependent conductivities of the specimens (Table 1.).

VII. Conclusion

Full waveform inversion was performed on GPR data recorded on concrete samples with different chloride contents and different humidities to investigate the influence on the relative permittivity and conductivity and to obtain quantitative values for the medium properties.

In general, the expected trends were verified with the inversion results, and showed that it is possible to discriminate the separate effects of chloride content and relative humidity on conductivity and relative dielectric permittivity. Chloride content has a more accentuated effect on wave propagation than relative humidity. However, some outliers need to be understood. An improved antenna calibration will probably enhance the inversion results.

Future work will focus on concrete specimens containing different chloride gradients and on the electromagnetic wave propagation model implementation for numerous layers to estimate these gradients.

VIII. Acknowledgment

REFERENCES

[1] J. Hugenschmidt, R. Loser, "Detection of chlorides and moisture in concrete structures with Ground penetrating radar", *Materials and Structures* 41:785-792, 2008

[2] S. Lambot, E.C. Slob, I. van den Bosch, B. Strockbroeckx, M. Vanclooster, "Modeling of Ground-Penetrating Radar for accurate characterization of subsurface electric properties" *IEEE Transactions on Geoscience and remote sensing*, vol. 42, pp. 2555-2568, Nov. 2004.

[3] S. Lambot, I. van den Bosch, B. Stockbroeckx, P. Druyts, M. Vanclooster, and E.C. Slob, "Frequency dependence of the soil electromagnetic properties derived from ground-penetrating radar signal inversion", Subsurface Sensing Technologies and Applications, Vol. 6 No. 1, 2005.

[4] Ernst, J.R., Maurer, H.R. Green, A.G., and Holliger K., "Full-waveform inversion of cross hole radar data based on 2-D finite difference time domain solutions of Maxwell's equations", IEEE Transactions on Geoscience and Remote Sensing, 45, 2807-2828.

[5] A.G. Meles, J.R. Ernst, J. van der Kruk, H.R. Maurer, A.G. Green, „New developments in FDTD full-waveform inversion of georadar data: a vectorial approach", in Proceedings of the 12th international conference on Ground Penetrating radar, Birmingham UK, 2008.

[6] A. Robert, "Dielectric permittivity of concrete between 50 Mhz and 1 Ghz and GPR measurements for building material evaluation" *Journal of Applied Geophysics*. 40:89-94, 1998.

[7] M.N. Soutsos.J.H. Bungey, S.G. Millard, M.R. Shaw, A. Patterson "Dielectric properties of concrete and their influence on radar testing" *NDT&E International*.34: 419-425, 2001.

[8] J. van der Kruk, R. Streich, A.G. Green, „Properties of surface waveguides derived from separate and joint inversion of dispersive TE and TM GPR data", Geophysics, v. 71, K19-K29, 2006.

[9] J.C. Lagarias, J.A. Reeds, M.H. Wright, and P.E. Wright, convergence properties of the Nelder-Mead simplex method in low dimensions, Society for Industrial and Applied Mathematics, 9, 1998.